IEEE Access
Multidisciplinary | Rapid Review | Open Access Journal

Received January 7, 2020, accepted January 25, 2020, date of publication February 13, 2020, date of current version February 25, 2020.

Digital Object Identifier 10.1109/ACCESS.2020.2973719

Compact Circularly Polarized Microstrip Ring Antenna Using Capacitive Coupling Structure for RFID Readers

SHIJI WU[1], JIADE YUAN[1], JIANGCHENG CHEN[2], AND YUJIE LI[1]

[1]College of Physics and Information Engineering, Fuzhou University, Fuzhou 350108, China
[2]Center for Wireless Communications–Radio Technologies Research Unit (CWC-RT), University of Oulu, 90570 Oulu, Finland

Corresponding author: Jiade Yuan (yuanjiade@fzu.edu.cn)

This work was supported in part by the Cooperation Project of Industry–University Research of Fujian Province, China, under Grant 2019H6007, and in part by the Science and Technology Project Plan of Fuzhou, China, under Grant 2018-G-89.

ABSTRACT This paper presents a compact circularly polarized microstrip antenna for radio frequency identification (RFID) readers. The dimensions of the proposed antenna are reduced by etching a cross slot in the radiation patch and loading four grounded coupling patches on the four corners of the radiation patch. An inverted Z-shaped coupling feedline is used to realize circularly polarized operation. The measured −10 dB $|S_{11}|$ bandwidth, 3-dB axial ratio bandwidth and maximum gain are 872−1095 MHz, 888−933 MHz, and 5.52 dBi, respectively, at 922 MHz frequency. The overall dimension of the proposed antenna is 0.36 $\lambda_g \times$ 0.36 $\lambda_g \times$ 0.05 λ_g (λ_g is the guide wavelength at the center frequency of 915 MHz). The proposed antenna has small size with good overall performance and is suitable for compact RFID devices.

INDEX TERMS Circular polarization (CP), coupling patch, coupling feedline, microstrip antenna, radio frequency identification.

I. INTRODUCTION

Radio frequency identification (RFID) is a wireless communication technology that uses electromagnetic waves to transmit and exchange information, and has been widely used in tracking of goods, manufacturing, supply chain, industry, and commerce. An RFID system typically includes a tag with product information and a reader receiving the information. Hence, the performance of reader antenna directly affects the RFID system [1].

Compact planar microstrip patch antennas are widely used in RFID systems because of their low profile, easy construction, and simple structure. Many techniques, such as using a substrate with high dielectric permittivity [2], slotting the radiation patch [3], and loading shorting probe [4], [5], have been developed to miniaturize microstrip antennas. Using a high dielectric permittivity substrate may be the effective means to reduce the size of antennas. However, these methods frequently lead to some negative effects, such as narrow bandwidth, high cost, and distorted antenna patterns. Circularly polarized reader antennas are usually required in RFID systems to avoid polarization mismatch between tags and readers, because RFID tag antennas are usually linearly polarized and randomly placed [6]. Theoretically, circularly polarized radiation can be obtained by exciting two orthogonal electric field components with equal amplitude and phase difference (PD) of 90°. Commonly used methods to obtain circularly polarized radiation mainly include multifed and single-fed methods. Multifed methods, such as 3-dB orthogonal branch coupler [7], [8], Wilkinson power splitter [9], 180° PD power splitter [10] and balun bandpass filter [11], can easily achieve circular polarization but need complicated feed networks. Single-fed techniques [12], [13] can also achieve circular polarization, although their design is difficult to implement because of their complex antenna structure with limited bandwidth.

In addition to miniaturization and circular polarization, high forward gain in certain environment and unidirectional radiation patterns are required in RFID reader antennas. A conducting plane can be placed as a reflector at a quarter wavelength distance from the radiator to achieve good unidirectional radiation for avoiding destructive interference between reflected and radiated waves [14]. However, the required quarter-wavelength profile height and large

The associate editor coordinating the review of this manuscript and approving it for publication was Qammer Hussain Abbasi.

reflector will result in a large antenna dimension. Many techniques have been proposed to reduce the distance between the radiator and the reflector for obtaining a unidirectional antenna with compact dimension. An artificial magnetic conductor (AMC) structure can reflect 0° phase over a finite frequency range, thereby reducing the profile height [15]. An electromagnetic bandgap structure provides a good directional radiation characteristic by suppressing surface wave propagation [16]. Frequency selective surface layers offer reflective phase coherence in broadband to achieve good antenna performance [17]. These techniques provide unidirectional radiation patterns although they experience the same problem, that is, the reflector structure is complex with extremely large size. Compared with [15]–[17], a simple resonance-based reflector structure is proposed to provide unidirectional radiation in broadband, but it cannot reduce the profile height [18], [19].

In this paper, a compact circular polarization unidirectional antenna for RFID readers is proposed. The antenna dimensions are reduced by etching a cross slot in the radiation patch to form a ring antenna and loading four grounded coupling patches on the four corners of the radiation patch. Circular polarization and wide bandwidth are realized using an inverted Z-shaped coupling feedline. The proposed antenna has smaller size, lower axial ratio (AR), and wider bandwidth compared with other microstrip structures with air gap [20], [21].

II. ANTENNA CONFIGURATION

As shown in Fig. 1(a), the proposed antenna consists of a radiation patch, a feedline, a ground plane and four small grounded coupling patches on the four corners, where the radiation patch and the feedline are printed on the upper and lower surfaces of the dielectric substrate. The dielectric substrate has a relative dielectric constant of 3.5, loss tangent of 0.0025, and thickness of 0.8 mm. The raw material of the ground and the four grounded patches are brass plate with a thickness of 0.3 mm. The upper dielectric substrate and the ground are separated by air with the height of h_1. As shown in Fig. 1(b), the square radiation patch is etched with a cross slot. The inverted Z-shaped coupling feedline is directly connected by the coaxial probe. As shown in Fig. 1(c), the four small grounded square patches are connected to the ground plane through the side grounding wall with the height of h_2.

The parameters of the proposed antenna are optimized on ANSYS HFSS 18. The optimized dimensions of the proposed antenna are listed in Table 1. The relevant design considerations and processes are discussed in detail.

III. ANTENNA DESIGN AND ANALYSIS

A. MINIATURIZATION ANALYSIS

The miniaturization of the proposed antenna is performed using three steps (Ants.1–3), as shown in the inset of Fig. 2. Ant.1 is a conventional square patch antenna fed by an inverted Z-shaped coupling feedline and resonated at the frequency of 3048 MHz. $|S_{11}|$ of Ant.1 is difficult to improve

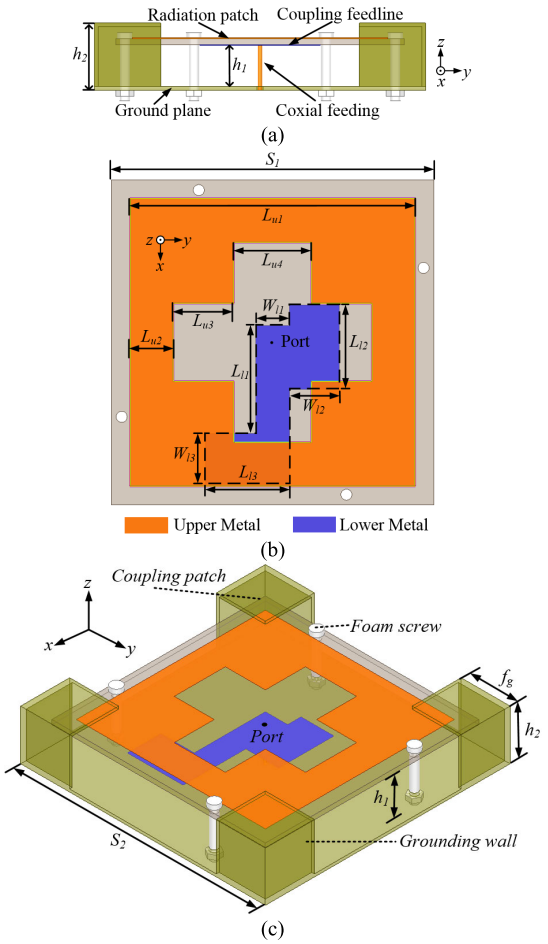

FIGURE 1. Geometry of the proposed antenna. (a) cross-sectional view, (b) top view (of slotted square patch), and (c) 3D view.

TABLE 1. Optimized geometric parameters (unit: mm).

Parameter	value	parameter	value	parameter	value
S_1	96	W_{l1}	10	L_{l3}	25
L_{u1}	85	L_{l1}	32	S_2	110
L_{u2}	13	W_{l2}	14.8	f_g	22
L_{u3}	18	L_{l2}	24.8	h_1	12
L_{u4}	23	W_{l3}	15	h_2	15

because of the lower profile height between the radiation patch and the ground plane. On the basis of Ant.1, a cross slot is etched in the center area of the radiation patch leading to a ring-shaped radiation patch of Ant.2. Thus, the resonant frequency of Ant.2 significantly decreases to 1793 MHz compared with that of Ant.1. This condition is because the side length of a ring patch antenna is approximately a quarter wavelength, which is half of the wavelength required by a conventional microstrip antenna. Four small grounded patches are symmetrically placed on the four corners to form Ant.3. The resonant frequency is decreased to 906 MHz compared with that of Ant.2 because of the introduction of coupling capacitance between the ground plane and the

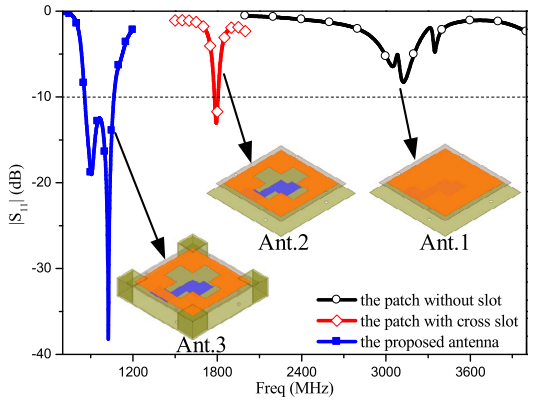

FIGURE 2. Simulated reflection coefficient of different structural evolutions.

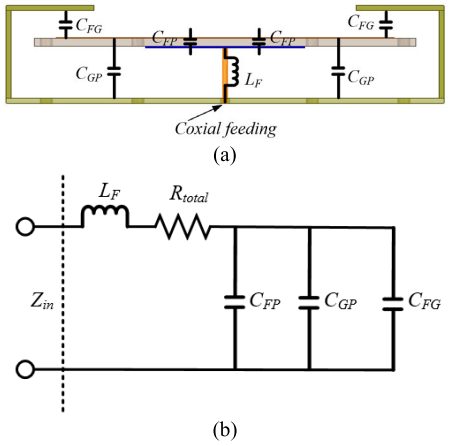

FIGURE 3. (a) Formation of equivalent capacitance and inductance, (b) equivalent circuit model for the proposed antenna.

ring patch. In other words, the introduction of a cross slot and four grounded patches can reduce the dimension of the antenna when the resonant frequency is to be maintained at 906 MHz, and Ant.3 has the smallest size among the three antennas. It can be seen in Fig. 2, the antenna size is reduced, and its impedance bandwidth is improved from Ants.1 to 3.

Fig. 3(a) shows the equivalent inductance and capacitance of the proposed antenna, where L_F and C_{FP} represent the inductance produced by the coaxial probe and the capacitance between the lower inverted Z-shaped coupling feedline and the upper radiation patch, respectively. C_{GP} and C_{FG} denote the capacitance between the ground plane and the radiation patch and between the radiation patch and the four small grounded coupling patches, respectively. R_{total} represent the total resistance including radiation dielectric, and equivalent resistance of the surface wave. Fig. 3(b) shows the equivalent circuit model of the proposed antenna. As described in [5], the total equivalent capacitance of the proposed structure by adding parallel C_{FP} and C_{FG} to the circuit model, can be expressed using the following equation:

$$C_{total} = C_{FP} + C_{GP} + C_{FG}. \quad (1)$$

Equation (1) indicates that the introduction of the capacitors of C_{FP} *and* C_{FG} can increase the total equivant capacitance of the proposed antenna, thereby reducing the resonant frequency on the basis of Cuircuit theory.

B. CIRCULAR POLARIZATION ANALYSIS

Circular polarization can be only achieved when two field components (i.e., $|E_y|$ and $|E_x|$) have equal in magnitude and their time PDs are odd multiple of 90°. Three feed structures are considered, namely Feed-1, Feed-2, and Feed-3, respectively, to explain the generation of circular polarization of the proposed antenna, as shown in Fig. 4. Feed-1 is a rectangular patch and symmetric about the x-axis. On the basis of Feed-1, a small rectangular patch is introduced and connected to the bottom left end of Feed-1 to form Feed-2. Another small rectangular patch is introduced and connected to the top right end of Feed-2 to form the Feed-3, thereby forming an inverted Z-shaped coupling feedline used in the proposed antenna.

Fig. 4(a) shows the two orthogonal far-field E_y and E_x amplitude ratios $|E_y/E_x|$ on the z-axis for the three feed structures. At the frequency range of 902−928 MHz, $|E_y/E_x|$ of Feed-1 is close to 0, which is a typical value of a linearly polarized antenna. This condition is because the antenna configuration is perfectly symmetric about Feed-1 in the x-axis direction, indicating that $|E_y/E_x|$ should be 0. $|E_y/E_x|$ of Feed-2 slightly deviates from 0 because the symmetry is destroyed by the connected small rectangular patch on the bottom left end of Feed-1. For Feed-3, $|E_y/E_x|$ in the frequency range is close to 1, indicating that the two far-field electric field components E_y and E_x are substantially equal in magnitude. Fig. 4(b) shows two orthogonal far-field E_y and E_x PDs for the three feed structures on the z-axis. At the frequency range of 902−928 MHz, the PDs of Feed-1 and Feed-2 are far from 90°, whereas Feed-3 PD is extremely close to 90°. The reason is that their varying lengths of W_{l2}, L_{l2}, W_{l3}, and L_{l3} produce different capacitance and control phases of the x-directed and y-directed current on the ring patch. As shown in Fig. 4(c), the AR of Feed-3 is less than 3 dB at the center frequency of 915 MHz.

To verify that the proposed antenna can generate circularly polarized radiation, the current density distributions on the ring-shaped radiation patch at different time instants are simulated and studied with the increase in time t from $\omega t = 0°$ to $\omega t = 270°$, as shown in Fig. 5. The resultant current at the frequency of 915 MHz points to the $+x$-direction, –y-direction, -x-direction and +y-direction, when $\omega t = 0°$, 90°, 180° and 270°, respectively. Thus, the resultant current vector sum flows in a clockwise direction. Therefore, the surface current distribution as a function of time mainly results in left-handed circular polarization (LHCP) radiation in the $z > 0$ half-space.

C. PARAMETRIC STUDIES

This section discusses some key parameters to clearly describe the antenna performance in terms of $|S_{11}|$ and AR. Only one geometric parameter is changed at a time unless

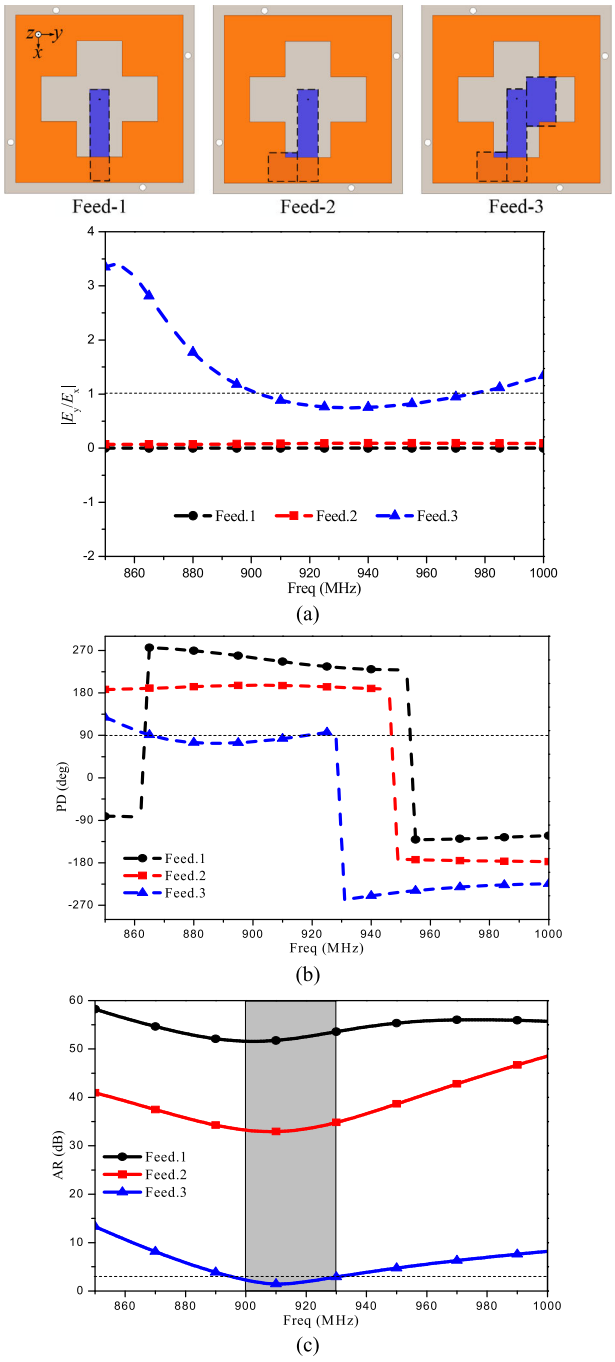

FIGURE 4. Simulation results of (a) amplitude ratios $|E_Y|/|E_X|$, (b) PDs, and (c) ARs of far-field component $|E_Y|$ and $|E_X|$ of the proposed antenna at the z-axis.

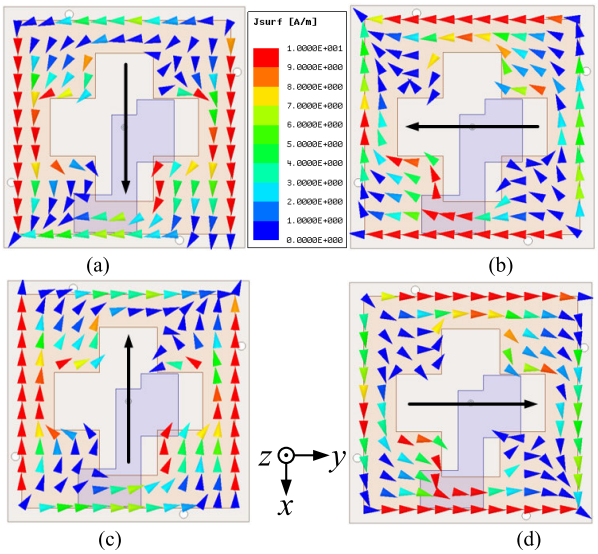

FIGURE 5. Simulated surface current distributions at the center frequency of 915 MHz. (a) $\omega t = 0°$ (or $t = 0$), (b) $\omega t = 90°$ (or $t = T/4$), (c) $\omega t = 180°$ (or $t = T/2$), and (d) $\omega t = 270°$ (or $t = 3T/4$). T is the period of the signal.

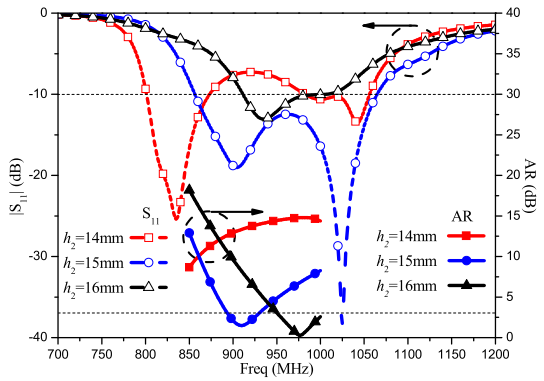

FIGURE 6. Variations of $|S_{11}|$ and AR with different dimensions of h_2.

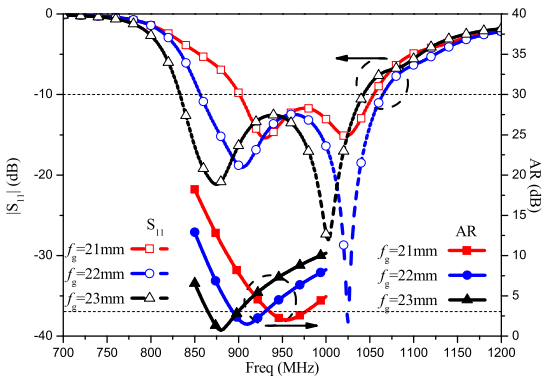

FIGURE 7. Variations of $|S_{11}|$ and AR with different dimensions of f_g.

otherwise specified, and the remaining geometric parameters remain unchanged.

Fig. 6 shows the effects of height (h_2) of the four grounded coupling patches on $|S_{11}|$ and AR. The resonant frequency shifts from the lower frequency to the higher one, and the impedance matching effectively increases first and then rapidly degrades when h_2 increases from 14 mm to 16 mm at steps of 1 mm. Similarly, AR is significantly improved first, and then the lowest value of AR shifts to the high frequency. This phenomenon occurs because the equivalent capacitance between the four grounded patches and the ring-shaped radiation patch is reduced with the increase in h_2.

The effects of side length (f_g) of the grounded coupling patch on $|S_{11}|$ and AR is shown in Fig. 7. The resonant frequency and the lowest values of AR shift to a lower frequency

TABLE 2. Comparison of antenna size and performance between the proposed and other existing antennas.

Refs.	−10 dB $\|S_{11}\|$ bandwidth, %	3-dB AR bandwidth, %	Max gain (dBi)	Permittivity	Physical dimension(λ_0^3)	Electrical dimension(λ_g^3)
[2]	2.453–2.534GHz, 3.3	2.484–2.501GHz, 0.68	3.8	10	0.18×0.18×0.03	0.55×0.55×0.08
[3]	2.384–2.445GHz, 2.5	2.402–2.414GHz, 0.5	4.3	3.38	0.29×0.29×0.01	0.53×0.53×0.02
[4]	1.563–1.590GHz, 1.7	1.570–1.580GHz, 0.63	5.4	3.5	0.47×0.47×0.02	0.88×0.88×0.03
[11]	2.36–2.47GHz, 4.55	/	5.9	3.55	0.65×0.65×0.04	1.21×1.21×0.08
[20]	3.17–3.77GHz, 17.3	/	8.2	Air	0.93×0.93×0.07	0.93×0.93×0.07
[21]	823–966MHz, 16	833–960MHz, 14.2	8	Air	0.60×0.60×0.14	0.60×0.60×0.14
This work	872–1095MHz , 22.7	888–933MHz , 4.9	5.52	Air	0.36×0.36×0.05	0.36×0.36×0.05

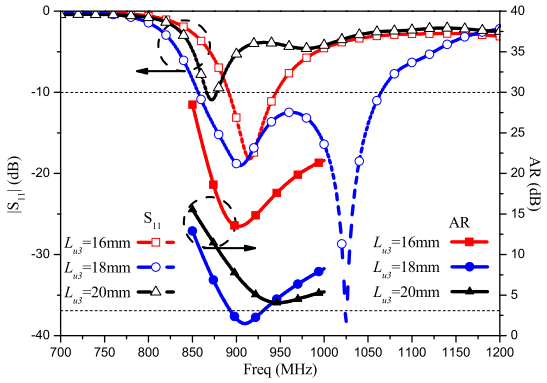

FIGURE 8. Variations of $|S_{11}|$ and AR with different dimensions of L_{u3}.

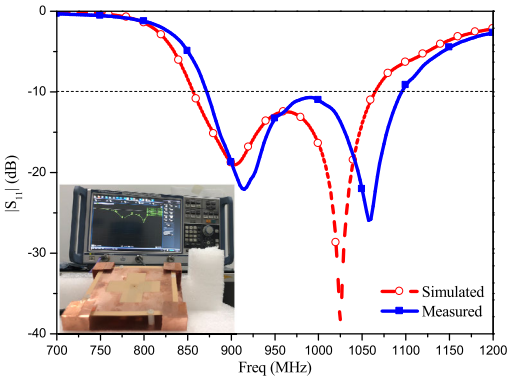

FIGURE 10. Simulated and measured $|S_{11}|$ of the proposed antenna.

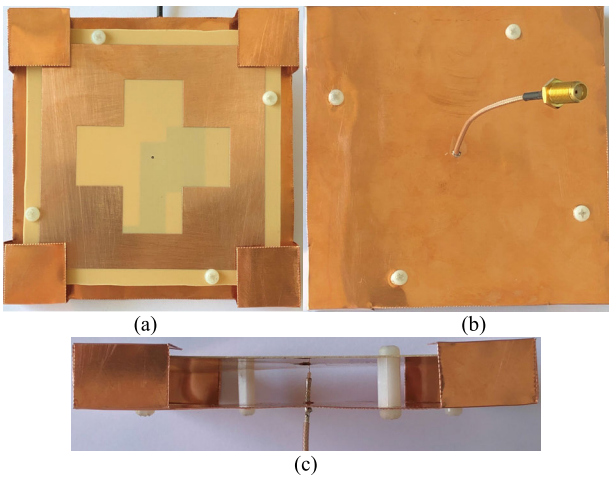

FIGURE 9. Fabricated prototype of the proposed antenna. (a) top view, (b) bottom view, and (c) side view.

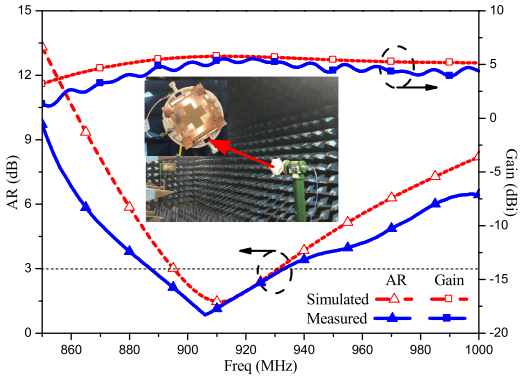

FIGURE 11. Simulated and measured AR and gain of the proposed antenna.

when f_g increases from 14 mm to 16 mm at steps of 1 mm. This finding is because the overlap area between the grounded coupling patches and the radiation patch increases with the increase in f_g, thereby increasing the equivalent capacitance between them.

As shown in Fig. 8, the effects of width (L_{u3}) of the cross slot in the radiation patch on $|S_{11}|$ and AR is studied. $|S_{11}|$ and AR become better and then worse when L_{u3} increases from 16 mm to 20 mm at steps of 2 mm. That is because the change in L_{u3} affects the coupling strength between the radiation patch and the inverted Z-shaped coupling feedline, resulting in significant variations of current distribution on the radiation patch.

IV. EXPERIMENTAL RESULTS AND DISCUSSIONS

The proposed antenna is fabricated on the basis of the final optimized antenna geometry parameters in Table 1. Figs. 9(a)-(c) show the top, bottom, and side views of the antenna prototype. Agilent E5071C vector network analyzer and microwave anechoic chamber are used to measure the electrical performance of the proposed antenna in terms of reflection coefficient $|S_{11}|$, AR, gain, and radiation pattern.

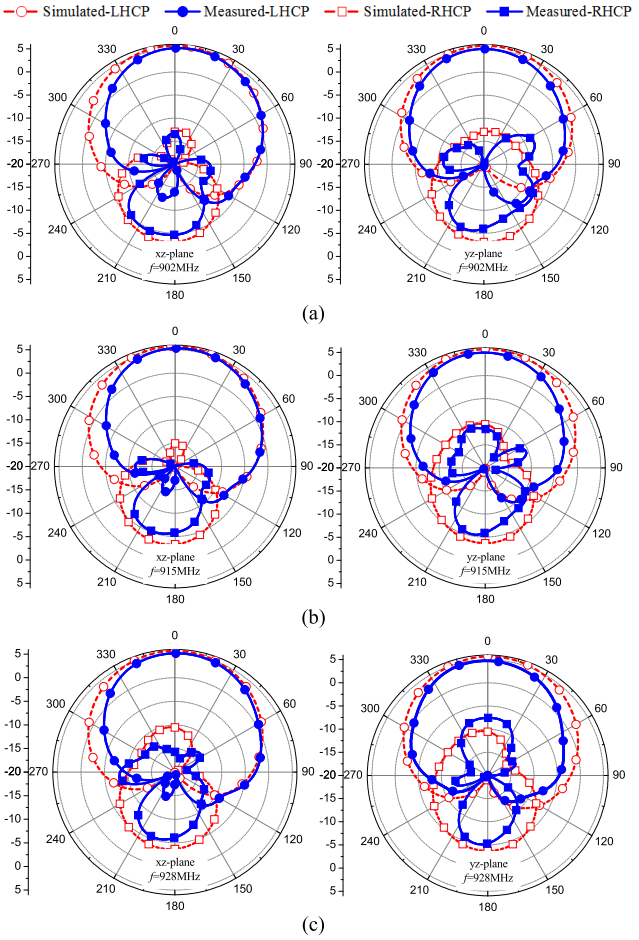

FIGURE 12. Simulated and measured radiation patterns at (a) 902 MHz, (b) 915 MHz, and (c) 928 MHz.

Fig. 10 shows the simulated and measured reflection coefficients. The simulated −10 dB $|S_{11}|$ bandwidth is 857−1064 MHz, whereas the measured bandwith is 872−1095 MHz. The simulated and measured results are in good agreement and both can completely cover the entire operating bandwidth of ultrahigh frequency (UHF) RFID.

Fig. 11 illustrates the simulated and measured curves of AR and gain at the boresight. The measured 3-dB AR bandwidth is 888−933 MHz, whereas the simulated AR bandwidth is 896−931 MHz. The measured results are in good agreement with the simulated results. The measured peak gain in the RFID operating band is 5.52 dBi.

Fig. 12(a–c) shows the measured and simulated radiation patterns in *xoz* and *yoz* planes at the frequencies of 902, 915, and 928 MHz, respectively. The measured gains at 902, 915, and 928 MHz are 5.22, 5.33, and 5.19 dBi, respectively. The simulated results are in reasonable agreement with the measured results. The difference between them is because of the manufacturing tolerances and errors between measurement and simulation.

Table 2 provides a comparison of antenna dimensions and other performances of the proposed antenna and previously published studies. It shows that the proposed antenna has wide impedance bandwidth and small electrical size.

V. CONCLUSION

This paper presents a compact circular polarization unidirectional antenna for RFID readers. The radiation patch of the proposed antenna is etched with a cross slot to form a ring antenna for reducing the antenna size. Four grounded coupling patches are placed on the four corners of the radiation patch to generate equivalent coupling capacitive reactance for further reducing the antenna size. Circular polarization and wide bandwidth are realized using the coupling feed of an inverted Z-shaped feedline. The measured −10 dB $|S_{11}|$ bandwidth, 3-dB AR bandwidth, and maximum gain in the operating frequency band of UHF RFID are 872–1095 MHz, 888–933 MHz and 5.52 dBi. The proposed antenna has the smallest size and maintains high unidirectional radiation gain compared with existing antennas, making it suitable for RFID readers.

REFERENCES

[1] X.-Z. Lai, Z.-M. Xie, Q.-Q. Xie, and X.-L. Cen, "A dual circularly polarized RFID reader antenna with wideband isolation," *IEEE Antennas Wireless Propag. Lett.*, vol. 12, pp. 1630–1633, 2013.
[2] H. Wong, K. K. So, K. B. Ng, K. M. Luk, C. H. Chan, and Q. Xue, "Virtually shorted patch antenna for circular polarization," *IEEE Antennas Wireless Propag. Lett.*, vol. 9, pp. 1213–1216, 2010.
[3] Nasimuddin, X. Qing, and Z. N. Chen, "Compact asymmetric-slit microstrip antennas for circular polarization," *IEEE Trans. Antennas Propag.*, vol. 59, no. 1, pp. 285–288, Jan. 2011.
[4] M.-S. Wang, X.-Q. Zhu, Y.-X. Guo, and W. Wu, "Compact circularly polarized patch antenna with wide axial-ratio beamwidth," *IEEE Antennas Wireless Propag. Lett.*, vol. 17, no. 4, pp. 714–718, Apr. 2018.
[5] J. Yuan, J. Zheng, and Z. D. Chen, "A compact meandered ring antenna loaded with parasitic patches and a slotted ground for global navigation satellite systems," *IEEE Trans. Antennas Propag.*, vol. 66, no. 12, pp. 6835–6843, Dec. 2018.
[6] Y.-F. Lin, C.-H. Lee, S.-C. Pan, and H.-M. Chen, "Proximity-fed circularly polarized slotted patch antenna for RFID handheld reader," *IEEE Trans. Antennas Propag.*, vol. 61, no. 10, pp. 5283–5286, Oct. 2013.
[7] J. Yuan, S. Wu, Z. Chen, and Z. Xu, "A compact low-profile ring antenna with dual circular polarization and unidirectional radiation for use in RFID readers," *IEEE Access*, vol. 7, pp. 128948–128955, 2019.
[8] J. Li, H. Liu, S. Zhang, Y. Zhang, and S. He, "Compact broadband circularly-polarised antenna with a backed cavity for UHF RFID applications," *IET Microw., Antennas Propag.*, vol. 13, no. 6, pp. 789–795, May 2019.
[9] J. Guo, J. Ouyang, Y. Yan, S. Zhang, and Z. Lu, "Compact circular polarization antenna based on slot structure for UHF RFID handheld reader," in *Proc. IEEE Int. Symp. Antennas Propag. USNC/URSI Nat. Radio Sci. Meeting*, Boston, MA, USA, Jul. 2018, pp. 331–332.
[10] Q. Liu, J. Shen, H. Liu, Y. Wu, M. Su, and Y. Liu, "Low-cost compact circularly polarized directional antenna for universal UHF RFID handheld reader applications," *IEEE Antennas Wireless Propag. Lett.*, vol. 14, pp. 1326–1329, 2015.
[11] H. Jin, G. Q. Luo, W. Che, K.-S. Chin, Y. Pan, and Y. Yu, "Vertically-integrated differential filtering patch antenna excited by a balun bandpass filter," *IET Microw., Antennas Propag.*, vol. 13, no. 3, pp. 300–304, Feb. 2019.
[12] Z. Wang, S. Fang, S. Fu, and S. Jia, "Single-fed broadband circularly polarized stacked patch antenna with horizontally meandered strip for universal UHF RFID applications," *IEEE Trans. Microw. Theory Techn.*, vol. 59, no. 4, pp. 1066–1073, Apr. 2011.
[13] J. Li, H. Liu, S. Zhang, M. Luo, Y. Zhang, and S. He, "A wideband single-fed, circularly-polarized patch antenna with enhanced axial ratio bandwidth for UHF RFID reader applications," *IEEE Access*, vol. 6, pp. 55883–55892, 2018.

[14] X. Fang, G. Wen, D. Inserra, Y. Huang, and J. Li, "Compact wideband CPW-fed meandered-slot antenna with slotted y-shaped central element for Wi-Fi, WiMAX, and 5G applications," *IEEE Trans. Antennas Propag.*, vol. 66, no. 12, pp. 7395–7399, Dec. 2018.
[15] J. Zhu, S. Li, S. Liao, and Q. Xue, "Wideband low-profile highly isolated MIMO antenna with artificial magnetic conductor," *IEEE Antennas Wireless Propag. Lett.*, vol. 17, no. 3, pp. 458–462, Mar. 2018.
[16] X. Yang, Y. Liu, Y.-X. Xu, and S.-X. Gong, "Isolation enhancement in patch antenna array with fractal UC-EBG structure and cross slot," *IEEE Antennas Wireless Propag. Lett.*, vol. 16, pp. 2175–2178, 2017.
[17] M. Borhani Kakhki, M. Mantash, A. Kesavan, M. M. Tahseen, and T. A. Denidni, "Millimeter-wave beam-tilting Vivaldi antenna with gain enhancement using multilayer FSS," *IEEE Antennas Wireless Propag. Lett.*, vol. 17, no. 12, pp. 2279–2283, Dec. 2018.
[18] S. A. Rezaeieh, M. A. Antoniades, and A. M. Abbosh, "Compact and unidirectional resonance-based reflector antenna for wideband electromagnetic imaging," *IEEE Trans. Antennas Propag.*, vol. 66, no. 11, pp. 5773–5782, Nov. 2018.
[19] L. Peng, J.-Y. Xie, X.-F. Li, and X. Jiang, "Front to back ratio bandwidth enhancement of resonance based reflector antenna by using a ring-shape director and its time-domain analysis," *IEEE Access*, vol. 5, pp. 15318–15325, 2017.
[20] L.-H. Wen, S. Gao, Q. Luo, Q. Yang, W. Hu, and Y. Yin, "A low-cost differentially driven dual-polarized patch antenna by using open-loop resonators," *IEEE Trans. Antennas Propag.*, vol. 67, no. 4, pp. 2745–2750, Apr. 2019.
[21] B.-S. Chen and C. Y. D. Sim, "Broadband circularly polarized stacked patch antenna for universal UHF RFID applications," in *Proc. ISAP*, Taiwan, China, Dec. 2014, pp. 99–100.

SHIJI WU was born in Ningde, Fujian, China, in 1993. He received the B.S. degree in communication engineering from the North China Institute of Science and Technology, Langfang, China, in 2017. He is currently with the Electronics and Communication Engineering Department, Fuzhou University, China. His current research interest includes antenna design and its applications for radio frequency identification (RFID) systems.

JIADE YUAN received the M.Sc. degree from the University of Electronic Science and Technology of China, in 2007, and the Ph.D. degree from the Nanjing University of Aeronautics and Astronautics, China, in 2010. Since 2013, he has been an Associate Professor with Fuzhou University, China. His current research interest includes antennas and microwave devices.

JIANGCHENG CHEN received the M.Sc. degree in communication engineering from The University of Manchester, U.K., in 2013. He is currently pursuing the Ph.D. degree with the Center for Wireless Communications, University of Oulu, Finland. He is also a Researcher with the Center for Wireless Communications, University of Oulu. His current research interests include wearable, 5G mobile terminal, THz integrated, and lens antennas.

YUJIE LI was born in Baoji, Shaanxi, China, in 1995. She received the B.S. degree in electronic science and technology from the Tianjin University of Technology, Tianjin, China, in 2017. She is currently pursuing the M.S. degree in electronics and communication engineering with Fuzhou University, China. Her current research interest includes antenna design and its applications for global navigation satellite systems.